Rare Metal Materials and Engineering
Volume 48, Issue 2, February 2019
Available online at www.rmme.ac.cn

Science Press

Cite this article as: Rare Metal Materials and Engineering, 2019, 48(2): 0440-0445.

ARTICLE

Effect of $Al_9Fe_{0.7}Ni_{1.3}$ Particle on the Microstructure and Mechanical Properties of Solution-treated Al-Zn-Mg-Cu-Ni Alloys Prepared by Spray Deposition

Liu Fei, Bai Pucun, Hou Xiaohu, Cui Xiaoming, Guo Ruixing

Inner Mongolia University of Technology, Hohhot 010051, China

Abstract: An Al-Zn-Mg-Cu alloy with Ni added as an alloying element was synthesized via spray deposition. The effects of the $Al_9Fe_{0.7}Ni_{1.3}$ particles on the microstructure and mechanical properties of the alloy after a solution treatment were investigated by scanning electron microscopy (SEM) in conjunction with electron backscatter diffraction (EBSD), transmission electron microscopy (TEM) and tensile tests. We find that the element Ni is present in the alloy in the form of spherical submicrometer $Al_9Fe_{0.7}Ni_{1.3}$ compound particles. The $Al_9Fe_{0.7}Ni_{1.3}$ compound particles are mainly distributed near the grain boundaries, revealing a powerful recrystallization inhibition effect during the solution treatment. After the solid solution treatment, the alloy exhibits an ultimate tensile strength of 603 MPa and an elongation of 11.79%, and transgranular ductile fracture is identified as the main fracture mechanism. The results show that the presence of the spherical submicrometer $Al_9Fe_{0.7}Ni_{1.3}$ compound particles plays a key role on the mechanical properties of the alloy, leading to grain refinement strengthening and Orowan strengthening, which is the main reason for the occurrence of transgranular ductile fracture.

Key words: $Al_9Fe_{0.7}Ni_{1.3}$; HRTEM; Al-Zn-Mg-Cu alloy; mechanical properties

Nickel, as a microalloying element, is currently used for the fabrication of Al-based alloys because of the formation of intermetallic compounds, which result in a significant improvement in the ageing precipitation behavior, the high-temperature mechanical strength, the frictional wear resistance and the stress corrosion cracking resistance[1-7]. However, some relatively coarse intermetallic particles can be formed during conventional solidification processes (slow cooling)[8-10]. This structural characteristic is unfavorable to the mechanical properties of these materials, and limits their application potential.

The spray deposition technique results in a rapid solidification, and has been used to produce Al alloy components with excellent properties. Using this technique, Silva et al[11] were able to prepare AlFeNi alloys with excellent mechanical properties, characterized by very fine (< 200 nm) and circular $Al_9(Fe, Ni)_2$ intermetallic compounds embedded within the Al matrix. Wang et al[12] reported an ultimate tensile strength of 695 MPa after a heat treatment for an Al-Zn-Mg-Cu alloy synthesized via spray deposition, which was composed of an Al matrix and submicron-sized $Al_9(Fe, Ni)_2$, Al_7Cu_2Fe intermetallic compounds. Many reports on the spray deposition of Ni-containing Al alloys mainly focused on the inter-relation between the microstructure and the mechanical properties of the supersaturated Al matrix and the precipitated phases[11, 13], but there have been very few studies which comprehensively considered the Ni-rich inter-metallic compounds' properties, size and distribution.

Moreover, various Ni-rich intermetallic compounds, which include Al_3Ni, $Al_{10}Fe_3Ni$, Al_3Ni_2, Al_7Cu_4Ni, Al_3CuNi and so on[10,14-17], have been found in synthesized Al alloys; among them the $Al_9(Fe, Ni)_2$ compound is usually observed in Ni-containing Al-Zn-Mg-Cu alloys[12,18]. However, the crystal structure of the $Al_9(Fe, Ni)_2$ phase remains controversial.

Received date: February 25, 2018
Foundation item: National Natural Science Foundation of China (11362014, 11672140); Research Program Supported by Inner Mongolia University of Technology (X201607); Graduate Research Innovation Project of Inner Mongolia Autonomous Region, China (B20171012808)
Corresponding author: Bai Pucun, Ph. D., Professor, College of Materials Science and Engineering, Inner Mongolia University of Technology, Hohhot 010051, P. R. China, Tel: 0086-471-6575790, E-mail: pcbai@163.com

Based on theoretical calculations combined with X-ray diffraction (XRD) analysis, Khiaidar et al[19] argued that $Al_9(Fe, Ni)_2$ was of the Co_2Al_9 structure and the $P2_1/3$ space group. Afterwards, the lattice parameters for this compound were determined by means of single-crystal XRD, as suggested by Chumak et al[16]. The results indicated that the $Al_9(Fe, Ni)_2$ compound has a monoclinic structure with lattice parameters a = 0.624 06 nm, b = 0.629 93 nm, c = 0.859 92 nm and β = 95.129°. Recently, however, based on selected area electron diffraction patterns, Wang et al[12] reported that the parameters of the $Al_9(Fe, Ni)_2$ compound were a = 0.8637 nm, b = 0.9000 nm, c = 0.8591 nm and β = 83.5°.

The aim of this study was thus to investigate the characteristics of the $Al_9(Fe, Ni)_2$ compounds in an Al12Zn2.4Mg1.1Cu0.5Ni alloy prepared via spray deposition, with an emphasis on the crystal structure. Subsequently, the effect of the particles' size and structure on the microstructure and mechanical properties of the alloy was assessed by means of scanning electron microscopy (SEM), transmission electron microscopy (TEM), tensile tests, and electron backscatter diffraction combined with energy-dispersive X-ray spectroscopy (EBSD-EDS).

1 Experiment

The alloy investigated in this study was synthesized through spray deposition in an Ospray OS10 (Ospray, UK) with a nominal composition (wt%) of 12Zn, 2.4Mg, 1.1Cu, 0.5Ni, 0.2Zr, balance Al. During the spray deposition process, the molten metal was atomized by an array of N_2 gas jets at 820 °C. The preform, named 'as-deposited sample', was heated at 407 °C and extruded to a round bar with a diameter of 50 mm. The extruded bar, named 'as-extruded sample', was then solution-treated at 485 °C for 2 h and water-quenched to room temperature (named 'solid-solution sample').

A Hitachi S3400 scanning electron microscope (Hitachi, Japan) equipped with a Deben microtest (2000 N) tensile test stage (Deben, UK) was used to determine the mechanical properties of the prepared alloy and to study the fracture surface. A tensile test specimen with a thickness of 1 mm was cut from the solid-solution sample by wire-cut electrical discharge machining. The dimensions of the prepared specimens are given in Fig.1. Each specimen was cut in such a way that its length direction was aligned parallel to the extruding direction of the bar. High-resolution transmission electron microscopy (HRTEM) and TEM investigations were performed on a JEM-2010 transmission electron microscope operated at 200 kV (JEOL, Japan). The TEM specimens were prepared by mechanical polishing followed by twin jet electropolishing. An FEI 650 field-emission SEM (FEI, USA) fully equipped for EBSD and EDS was used to map the locations of the grain boundaries and the distribution of the alloying elements. XRD test was performed to identify the phase composition using a Rigaku D/max 2500 X-ray diffractometer (Rigaku, Japan).

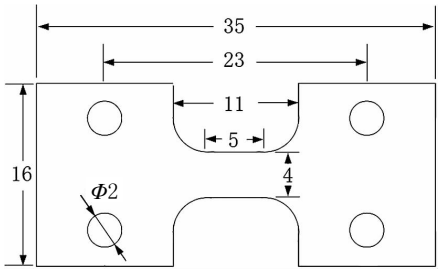

Fig.1 Schematic illustration of the tensile specimen (all dimensions in mm)

2 Results and Discussion

The X-ray diffraction (XRD) patterns obtained for the three types of samples (as-deposited, as-extruded and solid-solution) are presented in Fig.2. The comparison with the characteristic patterns in XRD databases, shown as insets in the bottom part of Fig.2, confirms that the as-deposited and the as-extruded samples mainly consist of an Al matrix and $MgZn_2$ and $Al_9(Fe, Ni)_2$ compounds. However, $MgZn_2$ is not detected in the solid-solution sample, which suggests that the $MgZn_2$ phase is largely dissolved into the Al matrix during the solution treatment at 485 °C and that the concentration of the residual $MgZn_2$ is too low to detect its presence.

The typical microstructure of the solid-solution samples is shown in the EBSD map in Fig.3a. The grain size is only about 15 μm. The corresponding element distribution maps are shown in Fig.3b~3h. We find three types of phases in the vicinity of the grain boundary: (i) a Cu-rich and Mg-rich phase, (ii) a Zr-rich phase, (iii) a Ni-rich and Fe-rich phase, exhibiting a typical recrystallization behavior inhibited by the secondary phases during the high-temperature heat treatment. In the Cu-rich and Mg-rich phase, according to the EDS analysis, the stoichiometric ratio of Cu to Mg is close to 1:1, and only a small amount of Zn is found in the phase apart from the Al matrix. Thus, this phase is considered to be the Al_2CuMg S-phase. However, no peak corresponding to this

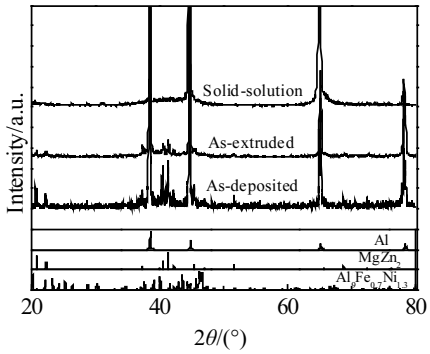

Fig.2 XRD patterns of the experimental alloy

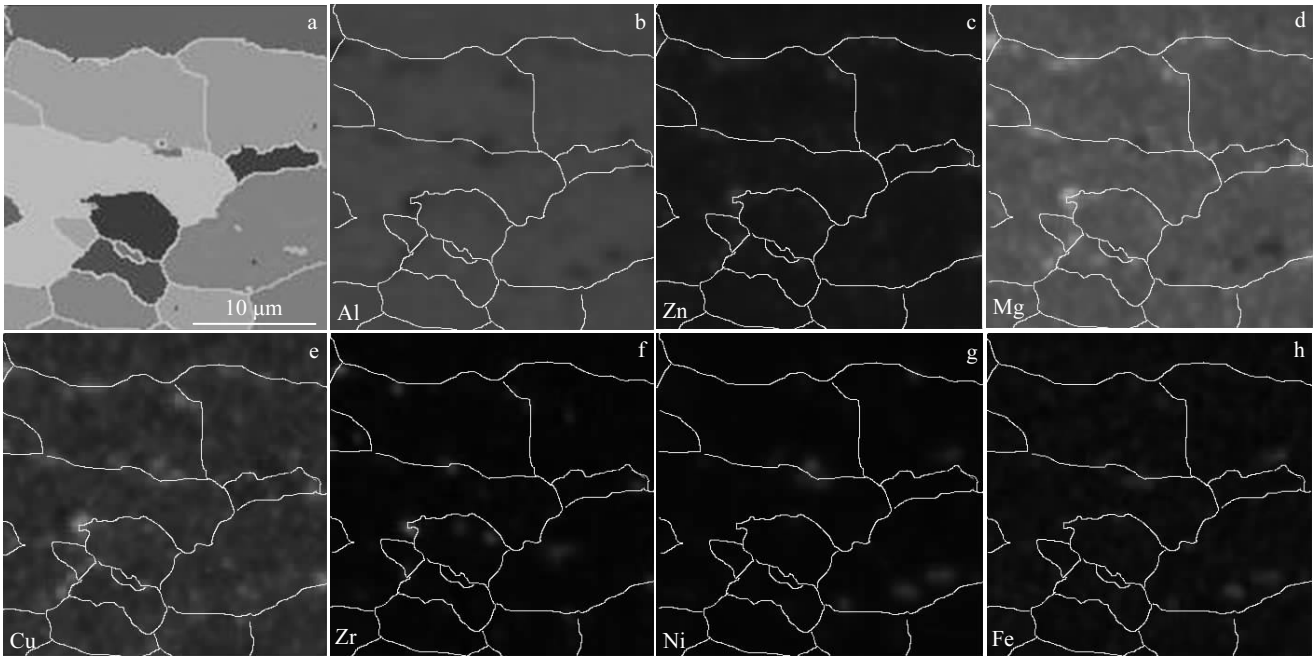

Fig.3 EBSD map (a) and element distribution maps obtained for the solid-solution sample: (b) Al, (c) Zn, (d) Mg, (e) Cu, (f) Zr, (g) Ni, and (h) Fe

phase is found in the XRD pattern because of the low concentration. The Zr-rich phase, with an approximate stoichiometric Al to Zr ratio of 3:1, is considered to be $L1_2$-Al_3Zr, which has the same crystal structure as the Al matrix. The presences of Al_2CuMg and $L1_2$-Al_3Zr in the Al-Zn-Mg-Cu alloy are in agreement with previous reports[20-24].

Fig.4a shows a spherical Ni-rich and Fe-rich particle with a diameter of about 700 nm. The corresponding HRTEM images of the particle are shown in Figs.4b~4d. The insets in the bottom left corner of Figs.4b~4d show the corresponding fast Fourier transform images. There are three types of HRTEM images with a different zone axis of the Ni-rich and Fe-rich phase. The results of the EDS analysis are shown in Fig.4e, indicating that the stoichiometric ratio of Al, Fe and Ni in the particle is close to 9:0.7:1.3. Thus, it is reasonable to assume that the Ni-rich and Fe-rich phase consists of $Al_9Fe_{0.7}Ni_{1.3}$. Chumak et al[16] reported that the $Al_9Fe_{0.7}Ni_{1.3}$ compound has a monoclinic structure with lattice parameters a=0.624 06 nm, b=0.629 93 nm, c=0.859 92 nm and β= 95.129° (ICSD No: 158246). Indexing of the FFT images (see insets in Fig.4b~4d) according to the crystal geometry and crystal diffraction pattern suggests that the Ni-rich and Fe-rich phase is of the same crystal structure as the $Al_9Fe_{0.7}Ni_{1.3}$ compound. Furthermore, the HRTEM micrographs of the particle were also compared with simulation results. The simulated images are overlaid with the HRTEM images and are depicted in Fig.5, shows that the simulated HRTEM images are in good agreement with the experimental observations. It further indicates that the Ni-rich and Fe-rich phase is the $Al_9Fe_{0.7}Ni_{1.3}$ phase.

Meanwhile, Fig.4a suggests that the $Al_9Fe_{0.7}Ni_{1.3}$ particle is attached to some Al_2CuMg phases (EDS result not listed here). This indicates that the $Al_9Fe_{0.7}Ni_{1.3}$ compounds can be regarded as the heterogeneous nucleation site for the Al_2CuMg phase during solidification.

To illustrate the effect of the $Al_9Fe_{0.7}Ni_{1.3}$ particles on the mechanical properties of the solid-solution samples, the fracture surface is presented in Fig.6. Compared with a spray-deposited Al-Zn-Mg-Cu-Zr alloy without Ni after the solution treatment, which shows a tensile strength of 510 MPa and an elongation at break of 12%[13], this solid-solution sample exhibits a higher tensile strength of 603 MPa, and a similar elongation at break of 11.79%. This suggests that the addition of Ni can greatly improve the strength while retaining the ductility of the alloy. In addition, the fracture surface exhibits a large number of dimples and shows the typical features of ductile fracture, indicating that transgranular fracture is the main fracture mechanism in the solid-solution samples. Moreover, the magnified image of the area marked black sqare in Fig.6a, shown in Fig.6b, reveals that there are some microcracks in the second-phase particles at the bottom of the dimples. This suggests that the second-phase particles became cracked during the tensile test due to the low ductility. The composition analysis confirms that those second-phase particles consisted of $Al_9Fe_{0.7}Ni_{1.3}$.

In general, the aim of the solution treatment is to dissolve most of the second-phase particles to enable the alloys to

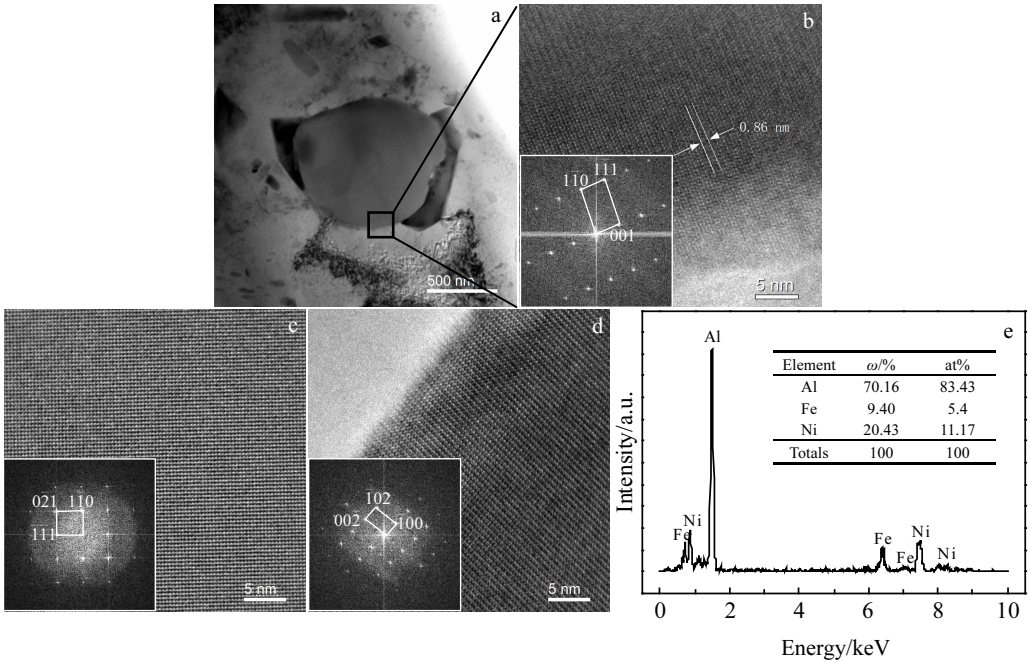

Fig.4 Analysis on an insoluble $Al_9Fe_{0.7}Ni_{1.3}$ particle with a diameter of 700 nm: (a) TEM image; (b~d) HRTEM images are from the [110], [112] and [010] zone axis of $Al_9Fe_{0.7}Ni_{1.3}$, respectively, with the insets at the bottom left corner of Fig.4b~4d showing the corresponding fast Fourier transforms of itself; (e) EDS result of the $Al_9Fe_{0.7}Ni_{1.3}$ particle

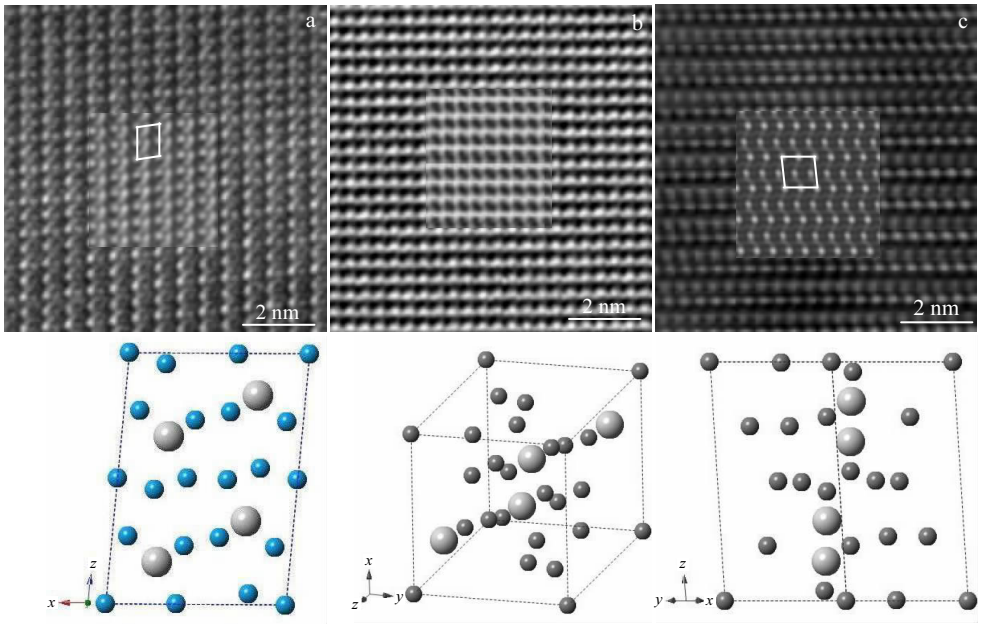

Fig.5 HRTEM images superimposed with the simulated images from the $Al_9Fe_{0.7}Ni_{1.3}$ structure with varying zone axis: (a) [010], (b) [112], and (c) [110] (the insets (bottom) are the corresponding projections of the structure consisting of Al (blue) as well as Fe/Ni (gray) atoms)

achieve their maximum strength in the subsequent aging treatment. For Al-Zn-Mg-Cu alloys, the second phases mainly include the η phase ($MgZn_2$), the S phase (Al_2CuMg) and the T phase ($Al_2Mg_3Zn_3$)[20,25]. The η, T and S phases can be dissolved at solution treatment temperatures of 470, 480 and 490 °C, respectively[26,27]. However, 470 °C is a common solution treatment temperature because a higher solution treatment temperature often results in recrystallization, which is detrimental to the mechanical properties of the alloys. In this study, the grains retained their small size after the solution

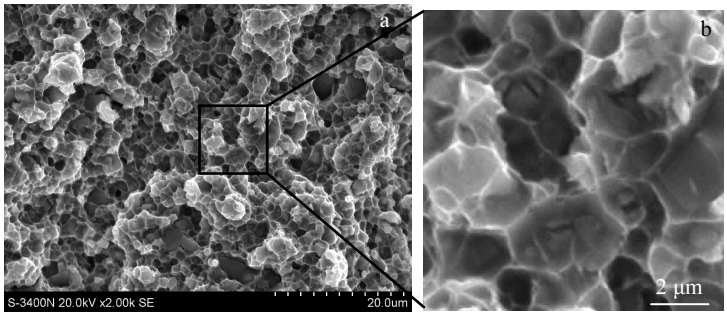

Fig.6 SEM images of the fracture surface

treatment at a temperature of 485 °C, and the $Al_9Fe_{0.7}Ni_{1.3}$ compound particles were found in the vicinity of the grain boundaries (Fig.3). These results show that the presence of the $Al_9Fe_{0.7}Ni_{1.3}$ compound particles can effectively inhibit recrystallization at higher temperatures and increase the degree of supersaturation of the alloying elements.

The effect of the $Al_9Fe_{0.7}Ni_{1.3}$ phase particles on the properties of the solid-solution samples can be explained by the following three mechanisms: (1) grain refinement strengthening: the yield strength of the alloys, σ, can be increased through grain size refinement, following the Hall–Petch relationship[28]:

$$\sigma = \sigma_0 + kd^{-1/2} \quad (1)$$

where σ_0 is the lattice friction stress for dislocation movement, k is a material constant, and d is the average grain size. Following Eq. (1), the increment in yield strength depends on the average grain size. According to the above analysis, the $Al_9Fe_{0.7}Ni_{1.3}$ compound particles are mainly located at the grain boundaries and lead to a typical recrystallization grain-growth inhibition effect (Fig.3). Consequently, this results in a grain refinement strengthening effect. (2) Orowan strengthening: moving dislocations will bypass the particles according to the Orowan mechanism when pinned by the particles. This will increase the resistance of the following moving dislocations, leading to high work hardening rates and a strengthening of the matrix[29]. (3) Ductility improvement: microcracks will form in the $Al_9Fe_{0.7}Ni_{1.3}$ particles due to the high stress concentration during the formation process owing to their limited ductility (Fig. 6). The microcracks can be considered as internal defects. According to the Griffith fracture criterion, the stress acting on an internal defect, σ_f, which is necessary to cause fracture, is given by

$$\sigma_f = \sqrt{\frac{2E\gamma_s}{\pi a}} \quad (2)$$

where E is Young's modules of the material, γ_s is the fracture surface energy, and a is the size of the existing microcrack[30] . In this work, the $Al_9Fe_{0.7}Ni_{1.3}$ compound particles have a submicron size (Figs.3 and 4), which means that they will be able to suffer a higher stress until fracture than those in conventional Al alloys, which contain relatively coarse intermetallic particles. Thus, the ductility can be improved by reducing the particles size. In conclusion, the addition of Ni to spray-deposited Al-Zn-Mg-Cu alloys leads to the formation of spherical submicrometer $Al_9Fe_{0.7}Ni_{1.3}$ compound particles, which greatly improves the strength while retaining the alloy's ductility.

3 Conclusions

1) Spherical submicrometer $Al_9Fe_{0.7}Ni_{1.3}$ compound particles of the $P2_1/3$ space group with lattice parameters a= 0.624 06 nm, b= 0.629 93 nm, c= 0.859 92 nm, β= 95.129° are formed during the spray deposition of Al-12Zn-2.4Mg-1.1Cu alloy when adding Ni (0.5 wt%).

2) Recrystallization grain-growth during the solution treatment is effectively inhibited by the $Al_9Fe_{0.7}Ni_{1.3}$ compound particles, which are located in the vicinity of the grain boundaries.

3) The mechanical properties of the alloy after the solid-solution treatment are greatly improved by the $Al_9Fe_{0.7}Ni_{1.3}$ compound particles, resulting in an ultimate tensile strength of 603 MPa and an elongation of 11.79%.

4) The main fracture mechanism of the prepared alloy is transgranular ductile fracture.

References

1 Yang C W, Chang Y H, Lui T S *et al*. *Materials & Design*[J], 2012, 40: 163

2 Tiwary C S, Kashyap S, Kim D H *et al*. *Materials Science and Engineering A*[J], 2015, 639: 359

3 Böyük U, Engin S, Maraşlı N. *Materials Characterization*[J], 2011, 62(9): 844

4 Casari D, Ludwig T H, Merlin M *et al*. *Materials Science and Engineering A*[J], 2014, 610: 414

5 Di Giovanni M T, Cerri E, Casari D *et al*. *Metallurgical and Materials Transactions A*[J], 2016, 47(5): 2049

6 Kundin J, Pogorelov E, Emmerich H. *Acta Materialia*[J], 2015, 83: 448

7 Naeem H T, Mohammed K S, Ahmad K R *et al*. *Digest Journal of Nanomaterials and Biostructures*[J], 2014, 9: 1309

8 Warmuzek M. *Journal of Alloys and Compounds*[J], 2014, 604:

245
9 Farkoosh A R, Pekguleryuz M. *Materials Science and Engineering A*[J], 2013, 582: 248
10 Elgallad E M, Shen P, Zhang Z *et al*. *Materials & Design*[J], 2014, 61: 133
11 Silva B L, Dessi J G, Gomes L F *et al*. *Journal of Alloys and Compounds*[J], 2017, 691: 952
12 Wang F, Xiong B Q, Zhang Y A *et al*. *Materials Science and Engineering A*[J], 2009, 518(1-2): 144
13 Wang F, Xiong B Q, Zhang Y A *et al*. *Materials & Design*[J], 2007, 28(4): 1154
14 Wang F, Xiong B Q, Zhang Y A *et al*. *Journal of Alloys and Compounds*[J], 2009, 487(1-2): 445
15 Yang Y, Yu K L, Li Y G *et al*. *Materials & Design*[J], 2012, 33: 220
16 Chumak I, Richter K W, Ipser H. *Intermetallics*[J], 2007, 15(11): 1416
17 MÖLler H, Stumpf W E, Pistorius P C. *Transactions of Nonferrous Metals Society of China*[J], 2010, 20(S3): 842
18 Mikhaylovskaya A V, Yakovtseva O A, Cheverikin V V *et al*. *Materials Science and Engineering A*[J], 2016, 659: 225
19 Khaidar M, Allibert C H, Driole J. *Zeitschrift fur Metall-kunde*[J], 1982, 73(7): 433
20 Liu B, Lei Q, Xie L Q *et al*. *Materials & Design*[J], 2016, 96: 217
21 Li G A, Zhang K, Lu Z *et al*. *Rare Metal Materials and Engineering*[J], 2016, 45(4): 1040 (in Chinese)
22 Shen Y G, Bai P C, Hou X H *et al*. *Rare Metal Materials and Engineering*[J], 2014, 43(8): 2032 (in Chinese)
23 Wen K, Xiong B Q, Zhang Y A *et al*. *Rare Metal Materials and Engineering*[J], 2017, 46(4): 928
24 Zhang J, Yang L, Zuo R L. *Rare Metal Materials and Engineering* [J], 2015, 44(4): 956 (in Chinese)
25 Yu H C, Wang M P, Jia Y L *et al*. *Journal of Alloys and Compounds*[J], 2014, 601: 120
26 Peng G S, Chen K H, Chen S Y *et al*. *Materials Science and Engineering A*[J], 2015, 641: 237
27 Yang X B, Chen J H, Liu J Z *et al*. *Materials Characterization*[J], 2013, 83: 79
28 Bazarnik P, Huang Y, Lewandowska M *et al*. *Materials Science and Engineering A*[J], 2015, 626: 9
29 Ma K, Wen H M, Hu T *et al*. *Acta Materialia*[J], 2014, 62: 141
30 Zhou D S, Qiu F, Jiang Q C. *Materials Science and Engineering A* [J], 2015, 622: 189

$Al_9Fe_{0.7}Ni_{1.3}$ 颗粒对固溶态喷射沉积 Al-Zn-Mg-Cu-Ni 合金组织和性能的影响

刘　飞，白朴存，侯小虎，崔晓明，郭瑞星
(内蒙古工业大学，内蒙古 呼和浩特 010051)

摘　要：利用喷射沉积技术制备含 Ni 的 Al-Zn-Mg-Cu 合金。利用扫描电镜和电子背散射衍射、透射电镜以及拉伸测试研究了 $Al_9Fe_{0.7}Ni_{1.3}$ 颗粒对合金固溶处理后组织和性能的影响。结果发现：合金中的 Ni 元素以亚微米球状 $Al_9Fe_{0.7}Ni_{1.3}$ 化合物的形式存在，$Al_9Fe_{0.7}Ni_{1.3}$ 颗粒主要在晶界附近分布，说明该颗粒在固溶过程中具有有力的抑制再结晶作用。固溶处理后，合金的抗拉强度为 603 MPa，断裂延伸率为 11.79%，主要断裂方式为穿晶延性断裂。实验结果表明，亚微米球状 $Al_9Fe_{0.7}Ni_{1.3}$ 化合物对合金性能有重要影响，可以产生细晶强化和 Orowan 强化，是合金发生穿晶延性断裂的主要原因。

关键词：$Al_9Fe_{0.7}Ni_{1.3}$；HRTEM；Al-Zn-Mg-Cu 合金；力学性能

作者简介：刘　飞，男，1986 年生，博士生，内蒙古工业大学材料科学与工程学院，内蒙古 呼和浩特 010051，电话：0471-6577161，E-mail: ngdliufei@163.com